J Electroceram (2008) 20:175–185
DOI 10.1007/s10832-007-9131-5

Spatial control of a smart beam

Omer Faruk Kircali · Yavuz Yaman · Volkan Nalbantoglu · Melin Sahin · Fatih Mutlu Karadal · Fatma Demet Ulker

Received: 2 December 2006 / Accepted: 11 April 2007 / Published online: 4 May 2007

Abstract This study presents the design and implementation of a spatial H_∞ controller for the active vibration control of a smart beam. The smart beam was modeled by assumed-modes method that results in a model including large number of resonant modes. The order of the model was reduced by direct model truncation and the model correction technique was applied to compensate the effect of the contribution of the out of range modes to the dynamics of the system. Additionally, spatial identification of the beam was performed, by comparing the analytical and experimental system models, in order to determine the modal damping ratios of the smart beam. Then, the spatial H_∞ controller was designed and implemented to suppress the first two flexural vibrations of the smart beam.

Keywords Smart beam · Assumed-modes method · Spatial system identification · Spatial H_∞ control

O. F. Kircali · Y. Yaman · V. Nalbantoglu · M. Sahin · F. M. Karadal
Department of Aerospace Engineering,
Middle East Technical University,
Ankara, Turkey

O. F. Kircali (✉)
STM Savunma Teknolojileri Muhendislik ve Ticaret A.S.,
Ankara, Turkey
e-mail: farukkircali@gmail.com

F. D. Ulker
Mechanical and Aerospace Engineering Department,
Carleton University,
Ottawa, Canada

1 Introduction

The vibration is an important phenomenon for the light-weight flexible aerospace structures. That kind of structures may be damaged under any undesired vibrational load. Hence, minimizing the structural vibration is necessary and this is achieved by means of a control mechanism. The usage of smart materials, as actuators and/or sensors, has given the opportunity to be used as a control mechanism.

The smart structure is a structure that can sense external disturbance and respond to that with active control in real time to maintain mission requirements [1]. Active vibration control of a smart structure requires an accurate system model of the structure. Modeling smart structures may require the modeling of both passive structure and the active parts. The governing differential equations of motion of the smart structures can be solved by analytical methods, such as assumed-modes method or finite element method [2]. Crawley and de Luis [3] presented an analytical modeling technique to show that piezoelectric actuators can be used to suppress some modes of vibration of a cantilevered beam. Caliskan [1] presented modeling of the smart structures by finite element modeling technique. Nalbantoglu [4] showed that experimental system identification techniques could also be applied on flexible structures to identify the system more accurately. The system model of a flexible structure has large number of resonant modes; however, general interest in control design is only on the first few ones. Hence, reducing the order of the system model is often required [5, 6]. A common approach is the direct model reduction. However, removing the higher modes directly from the system model perturbs the zeros of the system [7]. Therefore, in order to minimize the model reduction error, a correction term, including some of the removed modes, should be added to the truncated model [7, 8].

Today, robust stabilizing controllers designed in respect of H_∞ control technique are widely used on active vibration control of smart structures. Yaman et al. [9, 10] showed the effect of H_∞ controller on suppressing the vibrations of a smart beam due its first two flexural modes. Similar work is done for active vibration control of a smart plate, and usage of piezoelectric actuators on vibration suppression with H_∞ controller is successfully presented [11]. Ulker [12] showed that, beside the H_∞ control technique, μ-synthesis based controllers could also be successfully used to suppress the vibrations of smart structures.

Whichever controller design technique is applied, the suppression is preferred to be achieved over the entire structure rather than at specific points, since the flexible structures are usually distributed parameter systems. Moheimani and Fu [13] and Moheimani et al. [14] introduced spatial H_2 norm and H_∞ norm concepts in order to meet the need of spatial vibration control, and simulation based results of spatial vibration control of a cantilevered beam were presented. Moheimani et al. [14] studied spatial feedforward and feedback controller design, and presented illustrative results. They also showed that spatial H_∞ controllers could be obtained from standard H_∞ controller design techniques. Halim [15, 16] studied the implementation of spatial H_2 and H_∞ controllers on active vibration control and presented quite successful results. However these works were limited to a beam with simply-supported boundary condition.

This paper aims to present design and implementation of a spatial H_∞ controller on active vibration control of a cantilevered smart beam.

2 Modeling of the smart beam

Consider the cantilevered smart beam given in Fig. 1. The structural properties are given at Table 1. The smart beam consists of a passive aluminum beam (507×51×2 mm) with symmetrically surface bonded eight SensorTech BM500 type PZT (Lead-Zirconate-Titanate) patches (25×20×0.5 mm), which are used as actuators. The beginning and end locations of the PZT patches along the length of the beam are denoted as r_1 and r_2, where the patches are accepted as optimally placed [1]. The subscripts b and p indicate the beam and PZT patches, respectively. Note that, despite the actual length of the beam is 507 mm, the effective length reduces to 494 mm since it is clamped in the fixture.

Analytical modeling of the smart beam is performed by assumed-modes method, which represents the deflection of the beam by means of a series solution:

$$y(r,t) = \sum_{i=1}^{N} \phi_i(r) q_i(t) \tag{1}$$

where $\varphi_i(r)$ are admissible functions which satisfy the geometric boundary conditions of the passive beam, $q_i(t)$ are time-dependent generalized coordinates, r is the longitudinal axis and t is time. Assumed-modes method uses this solution to obtain approximate system model of the structure with the help of energy expressions [2]. The admissible functions are selected as the eigenfunctions of the passive cantilevered beam with the same structural properties as:

$$\phi_i(r) = L_b\{\cos h\beta_i r - \cos\beta_i r - \alpha_i(\sin h\beta_i r - \sin\beta_i r)\} \tag{2}$$

where

$$\alpha_i = \frac{\cos\beta_i L_b + \cos h\beta_i L_b}{\sin\beta_i L_b + \sin h\beta_i L_b} \tag{3}$$

where eigenfunctions satisfy the orthogonality conditions given below:

$$\int_0^{L_b} \rho_b A_b \phi_i(r)\phi_j(r)dr = \rho_b A_b L_b^3 \delta_{ij} \tag{4}$$

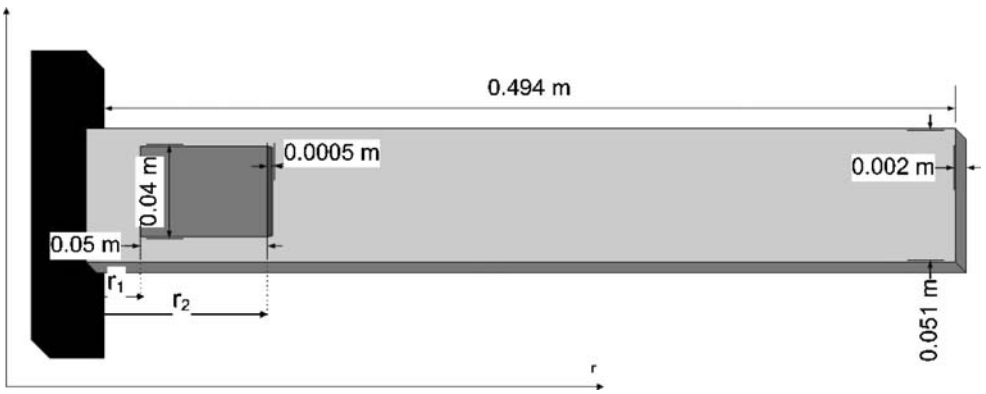

Fig. 1 The smart beam model used in the study

Table 1 Properties of the smart beam.

	Beam	PZT
Length, *m*	L_b=0.494	L_p=0.05
Width, *m*	w_b=0.051	w_p=0.04
Thickness, *m*	t_b=0.002	t_p=0.0005
Density, kg/m^3	ρ_b=2710	ρ_p=7650
Young's Modulus, *GPa*	E_b=69	E_p=64.52
Cross-sectional Area, m^2	A_b=1.02 10^{-4}	A_p=0.2 10^{-4}
Second Moment of Area, m^4	I_b=3.4 10^{-11}	I_p=6.33 10^{-11}
Piezoelectric charge constant, *m/V*	–	d_{31}=−175 10^{-12}

$$\int_0^{L_b} E_b I_b \frac{d^2\phi_i(r)}{dr^2}\frac{d^2\phi_j(r)}{dr^2}dr = \rho_b A_b L_b^3 \omega_i^2 \delta_{ij} \tag{5}$$

After some mathematical manipulations including the effect of PZT patches on passive beam [17], one can reach the input and output relation of the system dynamics as a transfer function from applied voltage to the deflection of the smart beam in the frequency domain as:

$$G_N(s,r) = \sum_{i=1}^{N} \frac{P_i\phi_i(r)}{s^2 + 2\xi_i\omega_i s + \omega_i^2} \tag{6}$$

Equation (6) implies the analytical system model of the smart beam shown in Fig. 1 including N number of resonant modes, where P_i is:

$$P_i = \frac{C_p\left[\phi_i'(r_2) - \phi_i'(r_1)\right]}{\{\rho A L^3\}_c} \tag{7}$$

where $\{\rho AL^3\}_c = \rho_b A_b L_b^3 + 2\rho_p A_p L_p^3$. The geometric constant $C_p = E_p d_{31} w_p\left(t_p + t_b\right)$ is related with the bending moment of PZT patches exerted on the beam [18].

3 Model correction

The analytical model of the smart beam consists of large number of resonant modes. However, in control design we deal with only the first few vibration modes of the smart beam. Hence, the full order model should be truncated to a lower order one. So the truncated model including first M number of modes can be expressed as:

$$G_M(s,r) = \sum_{i=1}^{M} \frac{P_i\phi_i(r)}{s^2 + 2\xi_i\omega_i s + \omega_i^2} \tag{8}$$

where M<<N. This truncation may cause error due to the removed higher order modes, which can be expressed as:

$$E(s,r) = G_N(s,r) - G_M(s,r) = \sum_{i=M+1}^{N} \frac{P_i\phi_i(r)}{s^2 + 2\xi_i\omega_i s + \omega_i^2} \tag{9}$$

In order to reduce the truncation error, a correction term should be added to the truncated model [8].

$$G_c(s,r) = G_M(s,r) + \sum_{i=M+1}^{N} \phi_i(r)k_i \tag{10}$$

where the optimal and general expression of constant k_i is [19]:

$$k_i^{opt} = \frac{1}{4\omega_c\omega_i}\frac{1}{\sqrt{1-\xi_i^2}}\ln\left\{\frac{\omega_c^2 + 2\omega_c\omega_i\sqrt{1-\xi_i^2} + \omega_i^2}{\omega_c^2 - 2\omega_c\omega_i\sqrt{1-\xi_i^2} + \omega_i^2}\right\}P_i \tag{11}$$

Consequently, the illustrative system models of the smart beam are shown in Fig. 2 for different points of interest along the beam. The full order model includes first 50 modes of the beam, i.e. N=50, whereas the truncated one includes only 2, i.e. M=2. The system is considered as undamped.

The magnitude of the frequency function shows the input output relation of the system, therefore it is unitless and presented as V_o/V_i, assuming V_o is the output voltage defined as the deflection of the beam measured by laser sensor and converted to a voltage value, and V_i is the input voltage to the system.

4 Spatial system identification

Experimental system identification, in collaboration with the analytical model, helps one to expose more accurate spatial characteristics of the structure. The frequency analysis lets one to obtain the transfer function of the

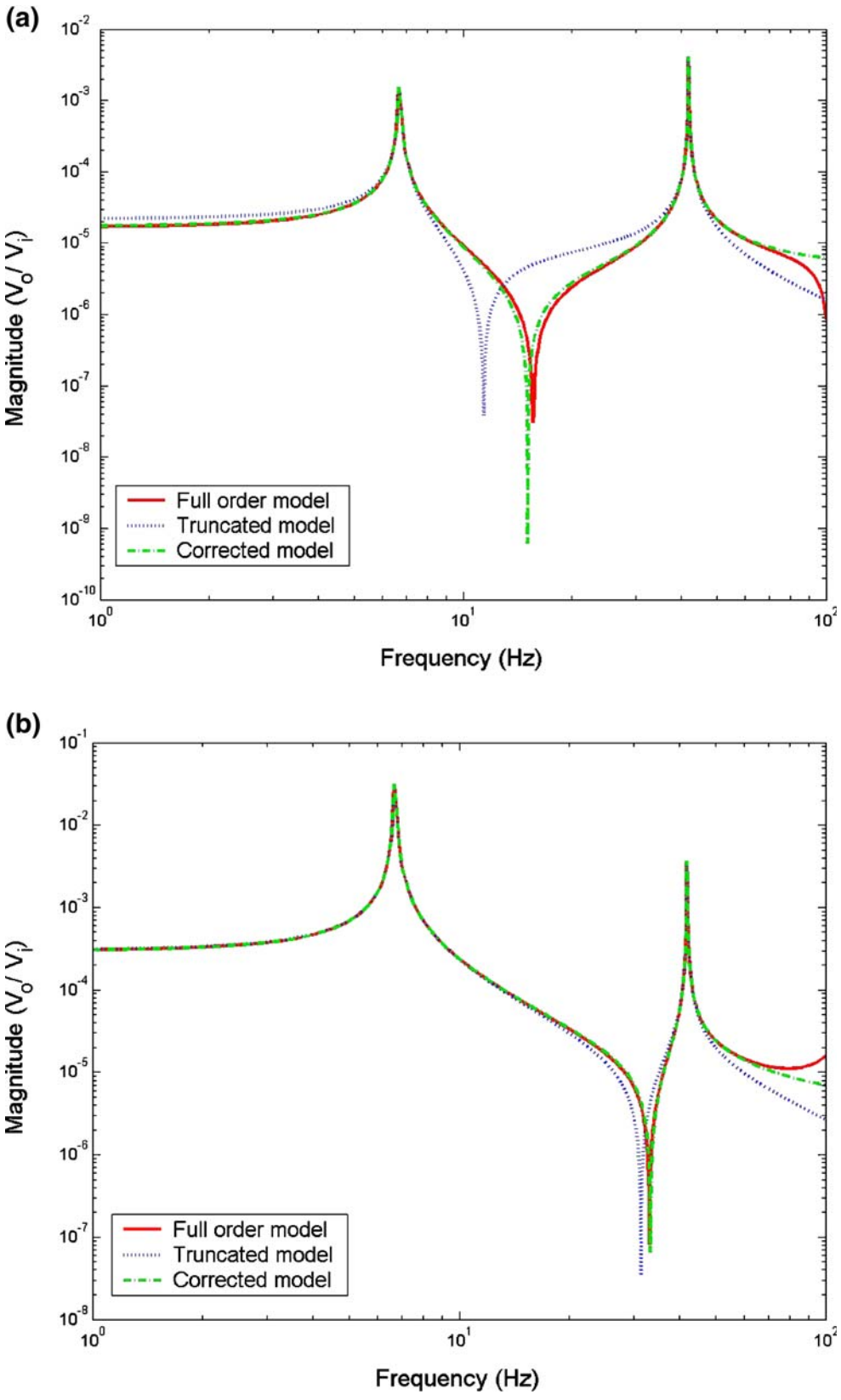

Fig. 2 Frequency response of the smart beam at (**a**) r=0.14 L_b. Frequency response of the smart beam at (**b**) r=0.75 L_b

Fig. 3 The smart beam used in the study

system [4] and clarify the resonance frequency values. Additionally, comparing the experimental model with the analytical one leads to determine the modal damping terms and the uncertainty on resonance frequencies [20].

Consider the smart beam of interest shown in Fig. 3, where the PZTs are used as the actuators and a Keyence LB-1201 (W) LB-300 laser displacement sensor is used as the sensor.

The smart beam was excited with sinusoidal chirp signal of amplitude 5 V within bandwidth 0.1–60 Hz, which covers first two flexural modes of the smart beam, and the response of the smart beam was acquired via laser displacement sensor from 17 different measurement points which are separated by 0.03 m interval from tip to root of the beam, i.e. 0.99 L_b, 0.93 L_b, ... etc. Assuming that the patches are relatively thin compared to the passive aluminum beam, our model can be considered as 1-D single input multi output system, where all the vibration modes are flexural modes. The experimental setup is shown in Fig. 4.

The applied voltage and the time response of the smart beam is shown in Fig. 5. The experimental and analytical models for 17 different measurement locations over the beam were compared and modal damping ratios were tuned till the magnitude of the analytical and experimental frequency responses at resonance frequencies match. As an example, the frequency responses for point r=0.93 L_b is shown in Fig. 6.

The uncertainty on resonance frequencies and modal damping ratios can also be determined by spatial system identification. There are different methods that can be applied to determine the uncertainty and improve the values of the parameters ω and ξ such as boot-strapping [21]. However, in this study we define the uncertainty as the standard deviation of the parameters. The final values of first two resonance frequencies and modal damping ratios of the smart beam are presented at Table 2.

5 Spatial H_∞ control of the smart beam

The spatial H_∞ control problem is to design a controller so as the ratio of the spatial energy of the system output to that of the disturbance signal is minimized [22]. Spatial H_∞ controllers could be obtained from standard H_∞ controller design technique [14]. Due to number of pages limitation, we will only present the results in this section and for more detailed explanation the reader is referred to reference [23].

Assume that, the disturbance is entering the system through the same channel as the controller output, the state-space representation of the system is:

$$\begin{aligned} \dot{x}(t) &= Ax(t) + B_1 w(t) + B_2 u(t) \\ y(t,r) &= \begin{bmatrix} \Pi \\ 0 \end{bmatrix} x(t) + \begin{bmatrix} \Theta_1 \\ 0 \end{bmatrix} w(t) + \begin{bmatrix} \Theta_2 \\ \kappa \end{bmatrix} u(t) \\ \tilde{y}(t,r_L) &= C_2 x(t) + D_3 w(t) + D_4 u(t) \end{aligned} \tag{12}$$

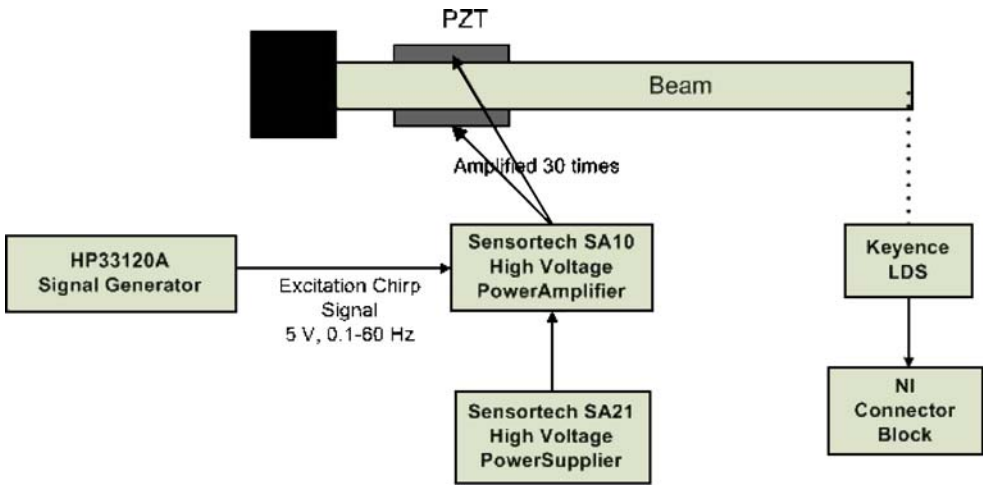

Fig. 4 Experimental setup for the spatial system identification of the smart beam

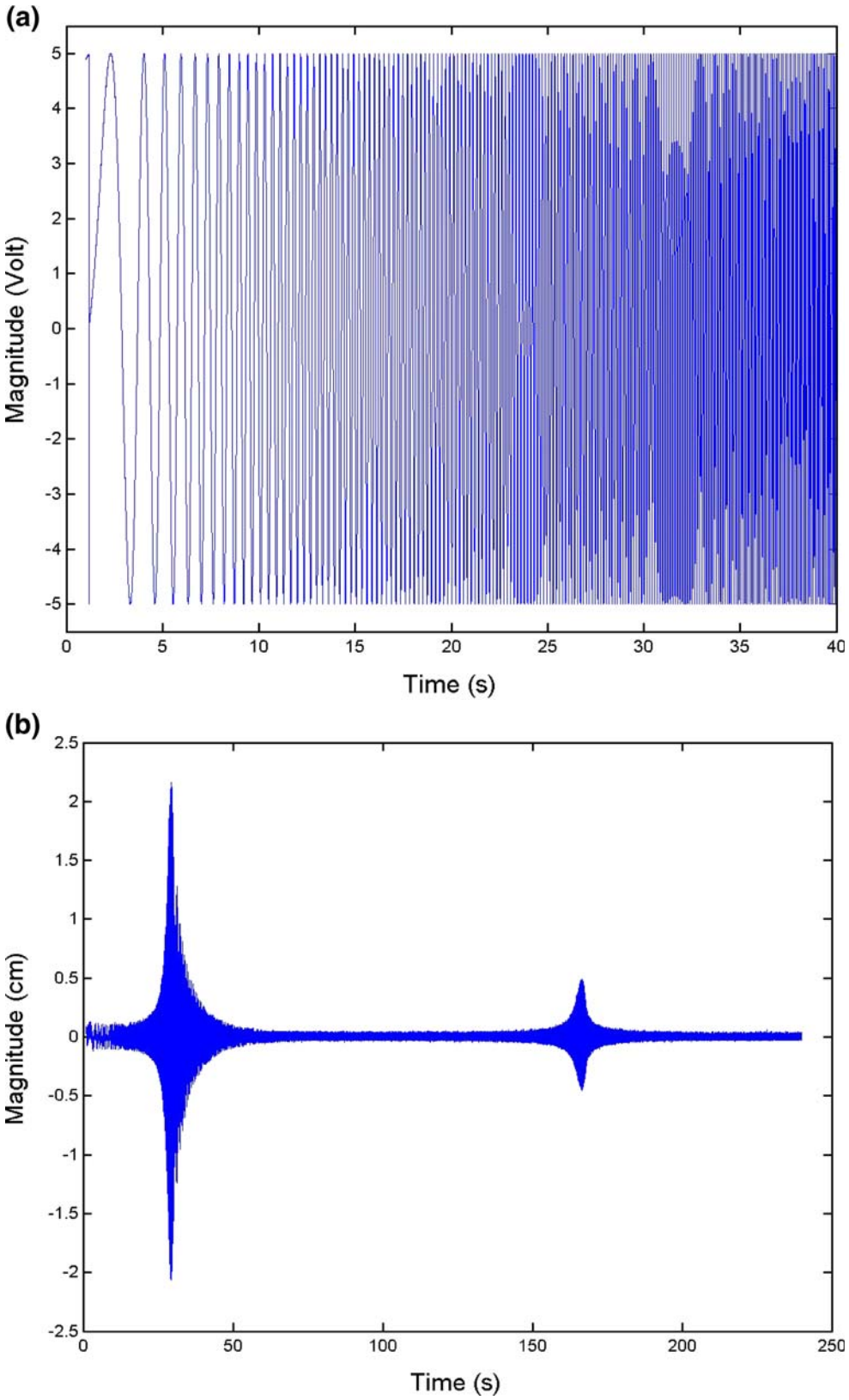

Fig. 5 (**a**) Applied voltage (**b**) Time response of the smart beam measured at r=0.99 L_b

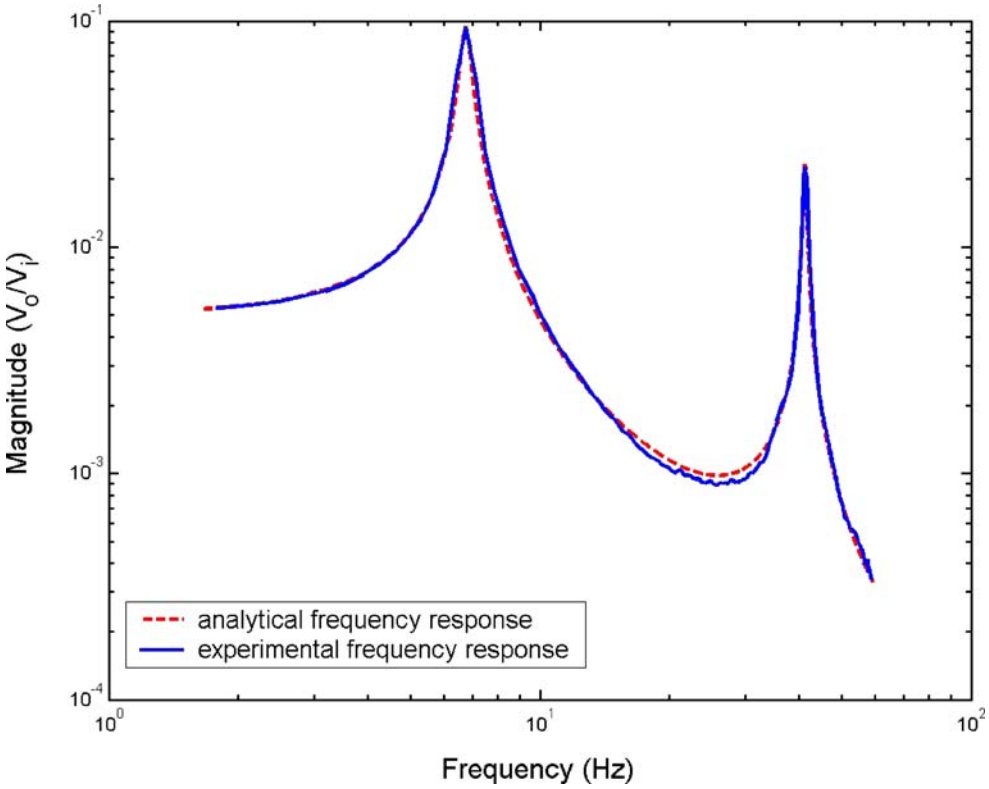

Fig. 6 Experimental and analytical frequency responses of the beam

where x is the state vector, w is the disturbance input, u is the control input, $y(r, t)$ is the performance output, $\widetilde{y}(t, r_L)$ is the measured output at location r_L=0.99 L_b, A is the state matrix, B_1 and B_2 are the input matrices from disturbance and control actuators respectively, Π is the output matrix of error signals, C_2 is the output matrix of sensor signals, Θ_1, Θ_2, D_3 and D_4 are the correction terms from disturbance actuator to error signal, control actuator to error signal, disturbance actuator to feedback sensor and control actuator to feedback sensor respectively and κ is the control weight designating the level of vibration suppression. Control weight prevents the controller having excessive gain and smaller κ results in higher level of vibration suppression. However, optimal value of κ should be determined in order not to neutrally stabilize the system. The state space representation variables are as follows:

$$A = \begin{bmatrix} 0_{2x2} & I_{2x2} \\ -\mathrm{diag}(\omega_1^2, \omega_2^2) & -\mathrm{diag}(2\xi_1\omega_1, 2\xi_2\omega_2) \end{bmatrix}, B_1 = B_2 = [0\ 0\ P_1 P_2]^T,$$

$$C_2 = [\phi_1(r_L)\phi_1(r_L)\ 0\ 0], D_3 = D_4 = \sum_{i=M+1}^{N} \phi_i(r_L) k_{ri}^{opt}$$

$$\Pi = \begin{bmatrix} L_b^{3/2} & 0 & 0 & 0 \\ 0 & L_b^{3/2} & 0 & 0 \\ 0 & 0 & 0 & 0 \\ 0 & 0 & 0 & 0 \\ 0 & 0 & 0 & 0 \end{bmatrix}, \Theta_1 = \Theta_2 = \begin{bmatrix} 0 & 0 & 0 & 0 & \sqrt{\sum_{i=M+1}^{N} L_b^3 \left(k_{ri}^{opt}\right)^2} \end{bmatrix}^T$$

Control weight κ is selected as 7.87×10^{-7}. Note that the size of the state space variables strictly depend on the order of the truncated model, e.g. in our case M=2 so the size of state matrix A is 4×4. The experimental setup for implementation of spatial controller is shown in Fig. 7. Firstly, the free vibration suppression of the smart beam is studied. The smart beam is given an initial 5 cm tip deflection and the suppression of the free vibration of the smart beam is presented in Fig. 8. Then, the forced vibration suppression of the smart beam is conducted. The forced vibration control of the smart beam was analyzed in two different configurations. In the first

Table 2 Mean and standard deviation of the first two resonance frequencies and modal damping ratios.

	ω_1(Hz)	ω_2(Hz)	ξ_1	ξ_2
Mean	6.742	41.308	0.027	0.007
Standard Deviation	0.009	0.166	0.002	0.001

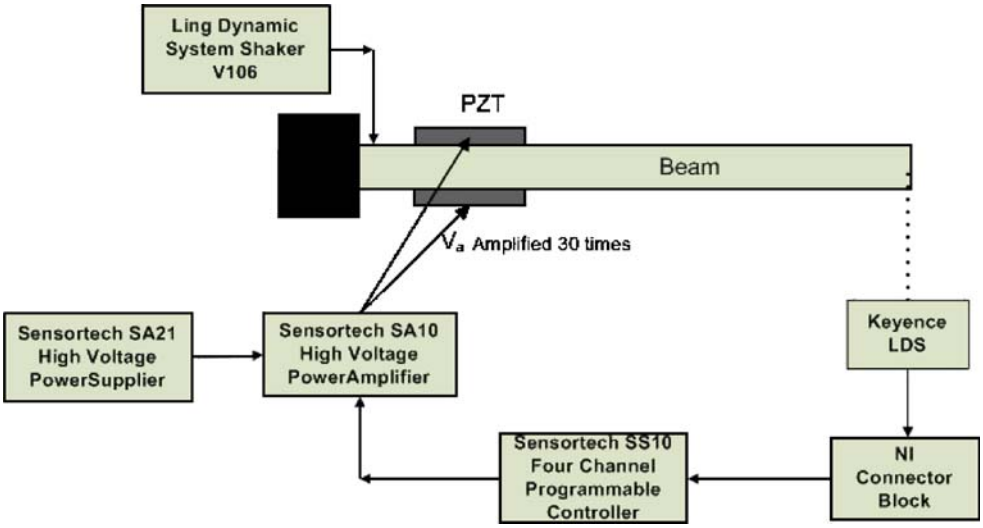

Fig. 7 Experimental setup for control of the smart beam

one, the smart beam was excited for 180 s with a shaker located very close to the root of the smart beam, on which a sinusoidal chirp signal of amplitude 4.5 V was applied. The excitation bandwidth was taken as first 5–8 Hz and later 40–44 Hz including the first two resonance frequencies separately. The open loop and closed loop frequency responses of the smart beam under corresponding excitations are shown in Fig. 9. In the second configuration, instead of using a sinusoidal chirp signal, constant excitation at the resonance frequencies was applied for 20 s via shaker. The open loop and closed loop time responses of the smart beam were measured and shown in Fig. 10.

6 Conclusion

In this paper, the design and implementation of a spatial H_∞ controller was presented for suppressing the first two

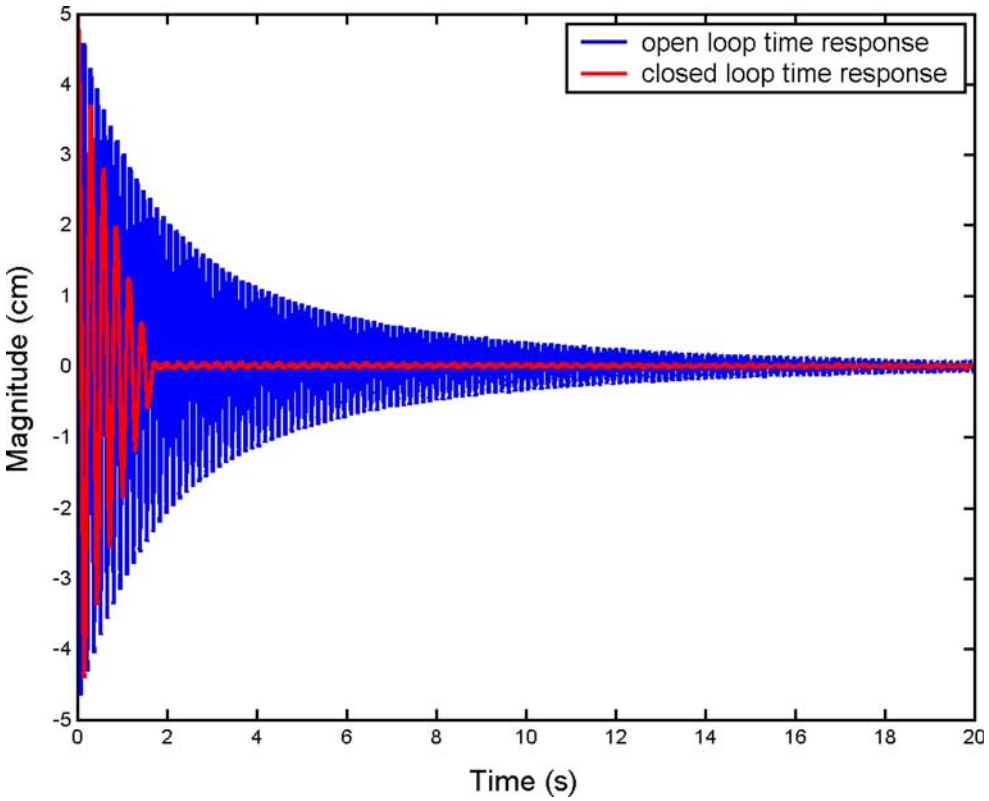

Fig. 8 Free vibration of the smart beam

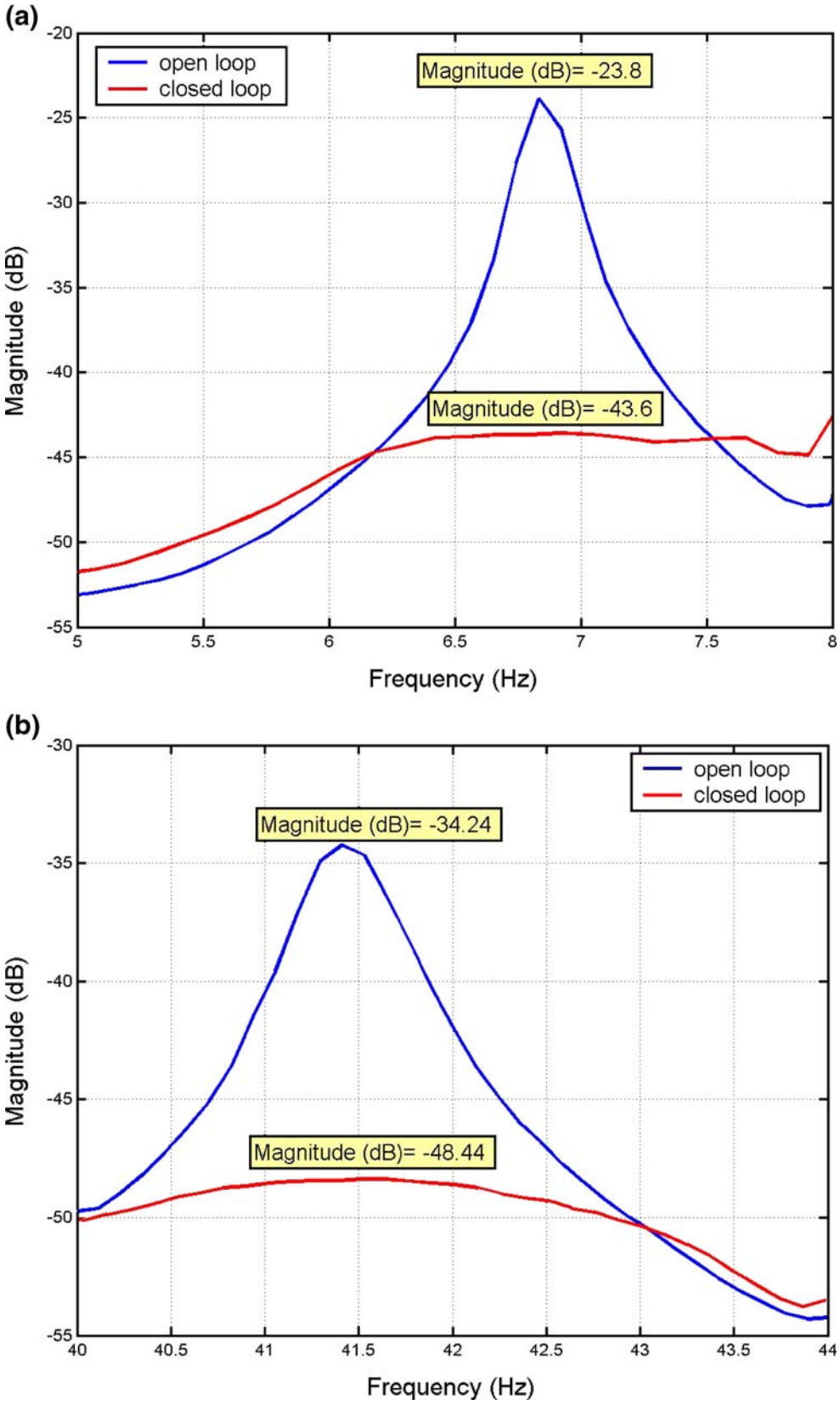

Fig. 9 Frequency responses of the open loop and closed loop systems within excitation of (**a**) 5–8 Hz (**b**) 40–44 Hz

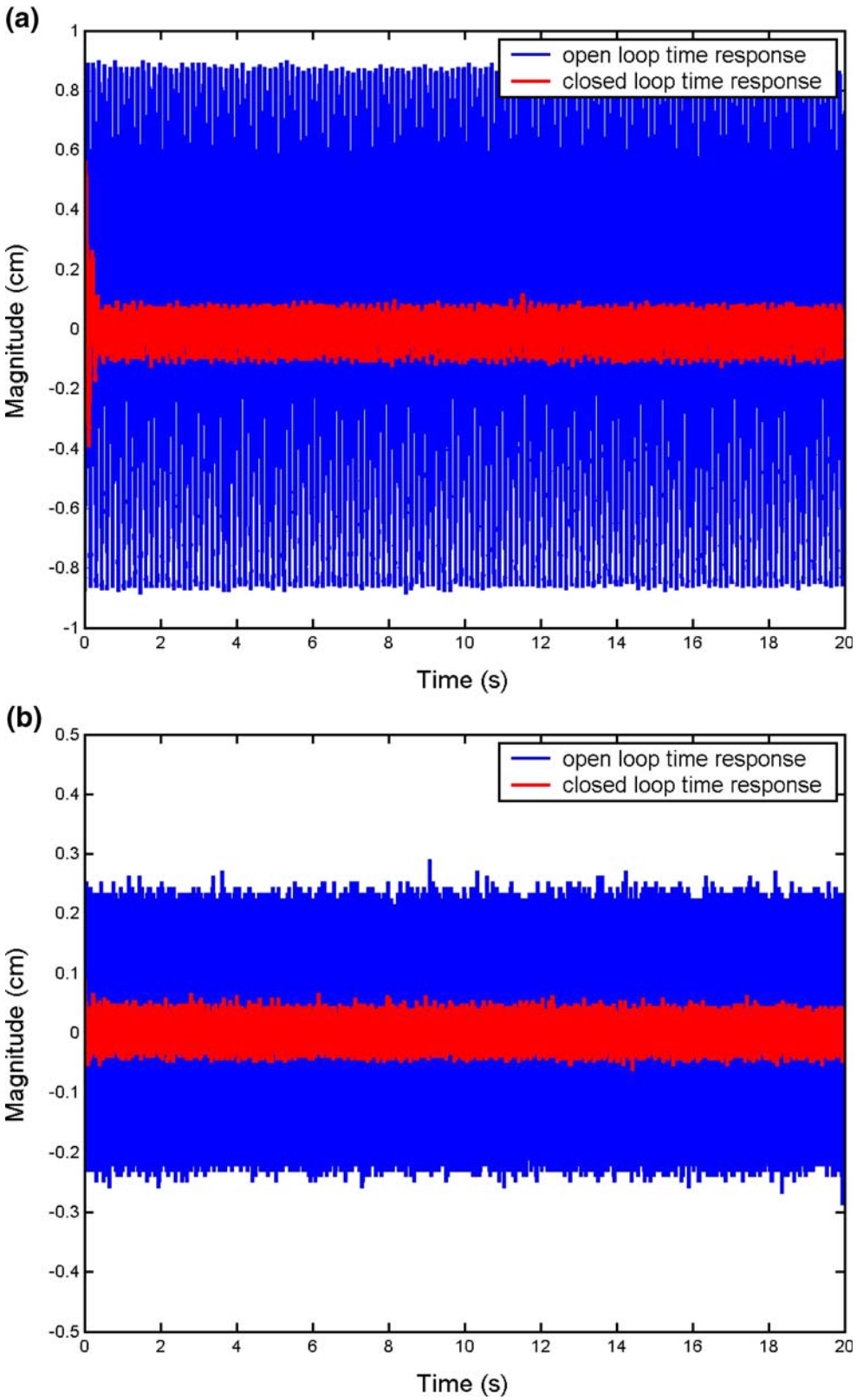

Fig. 10 Open and closed loop time responses of the smart beam under constant excitation at (**a**) first resonance frequency (**b**) second resonance frequency

flexural vibrations of a smart beam. The system model of the smart beam was obtained analytically and then improved experimentally. The free and forced vibrations of the smart beam were suppressed successfully.

References

1. T. Caliskan, PhD Thesis, Middle East Technical University, (2002)
2. L. Meirovitch, *Elements of Vibration Analysis* (McGraw-Hill, 1986)
3. E.F. Crawley, J. Louis, AIAA J. **125**(10), 1373–1385 (1989)
4. V. Nalbantoglu, Ph.D. Thesis, University of Minnesota, (1998)
5. P.C. Hughes, R.E. Skelton, J. Guid. Control **4**(3), (1981)
6. S.O.R. Moheimani, H.R. Pota, I.R. Petersen, *Proceedings of the American Control Conference* (Albuquerque, New Mexico, June 1997), pp. 3098–3102
7. R.L. Clark, Trans. ASME: J. Dyn. Syst. Meas. Control **119**, 390–395 (1997)
8. S.O.R. Moheimani, Trans. ASME: J. Dyn. Syst. Meas. Control **122**, 237–239 (2000)
9. Y. Yaman, T. Caliskan, V. Nalbantoglu, E. Prasad, D. Waechter, B. Yan, *Canada–US CanSmart Workshop on Smart Materials and Structures, Canada Proceedings* (Montreal, 2001), pp. 137–147
10. Y. Yaman, F.D. Ulker, V. Nalbantoglu, T. Caliskan, E. Prasad, D. Waechter, B. Yan, *AED2003, 3rd International Conference on Advanced Engineering Design*, Paper A5.3, (Prague, Czech Republic, 01-04, 2003), pp. 137–147
11. Y. Yaman, T. Caliskan, V. Nalbantoglu, F.D. Ulker, E. Prasad, D. Waechter, B. Yan, *ESDA2002, 6th Biennial Conference on Engineering Systems Design and Analysis*, Paper APM-018, (Istanbul, Turkey, 2002), July 8–11
12. F.D. Ulker, M.S. Thesis, Middle East Technical University, (2003)
13. S.O.R. Moheimani, M. Fu, *International Proceedings of 37th IEEE Conference on Decision and Control* (Tampa Florida, USA, 1998)
14. S.O.R. Moheimani, I.R. Petersen, H.R. Pota, J Sound Vib. **227**(4), 807–832 (1999)
15. D. Halim, S.O.R. Moheimani, IEEE Trans. Control Syst. Technol. **10**(4), (2002)
16. D. Halim, S.O.R. Moheimani, IEEE/ASME Trans. Mechatron. **7**(3), (2002)
17. O.F. Kircali, Y. Yaman, V. Nalbantoglu, M. Sahin, F.M. Karadal, *VI. Aeronautics Symposium* (12–14 May 2006, Nevsehir, Turkey), pp. 164–168 (in Turkish)
18. H.R. Pota, T.E. Alberts, in *Proceeding IEEE International Conference on Systems Engineering* (Japan, September 1992)
19. D. Halim, PhD. Thesis, School of Electrical Engineering and Computer Science, University of Newcastle, (2002)
20. W. Reinelt, S.O.R. Moheimani, in *Proceedings of the 8th International Mechatronics Conference* (Enschede, Netherlands, 2002)
21. O.F. Kircali, Y. Yaman, V. Nalbantoglu, M. Sahin, F.M. Karadal, F.D. Ulker, *VI. Aeronautics Symposium* (12–14 May 2006, Nevsehir, Turkey), pp. 247–251 (in Turkish)
22. S.O.R. Moheimani, D. Halim, A.J. Fleming, *Spatial Control of Vibration. Theory and Experiments* (World Scientific, 2003)
23. O.F. Kircali, M.S. Thesis, Middle East Technical University, (2006)